

# The development of biofilm architecture

A. C. Fowler<sup>1,2</sup>, T. M. Kyrke-Smith<sup>3</sup>, and H. F. Winstanley<sup>1</sup>

<sup>1</sup>MACSI, University of Limerick, Limerick, Ireland

<sup>2</sup>OCIAM, University of Oxford, Oxford, UK

<sup>3</sup>British Antarctic Survey, Cambridge, U. K.

March 15, 2016

## Abstract

We extend the one-dimensional polymer solution theory of bacterial biofilm growth described by Winstanley *et al.* (2011) to deal with the problem of the growth of a patch of biofilm in more than one lateral dimension. The extension is non-trivial, as it requires consideration of the rheology of the polymer phase. We use a novel asymptotic technique to reduce the model to a free-boundary problem governed by the equations of Stokes flow with non-standard boundary conditions. We then consider the stability of laterally uniform biofilm growth, and show that the model predicts spatial instability, and this is confirmed by a direct numerical solution of the governing equations. The instability results in cusp formation at the biofilm surface, and provides an explanation for the common observation of patterned biofilm architectures.

*Keywords:* Biofilm architecture, instability, biofilm structure, biofilm pattern.

## 1 Introduction

Bacterial biofilms are virtually ubiquitous. In a biofilm, bacterial cells attach to one another – and usually to a surface or interface – with a slime matrix which largely immobilises the cells and creates a distinct micro-environment. Combined with associated phenotypic changes, this provides a measure of protection from physical and chemical attack which allows biofilm to persist in even the most extreme environments (Whitman *et al.* 1998). This resistance also makes biofilm a major consideration in many applications of human interest, with both positive effects (biogeochemical cycles, gut flora, wastewater treatment, bioreactors) and negative (medical devices, pathology, industrial fouling and corrosion).

While early mathematical models of biofilm implicitly assumed that it forms a uniform, smooth layer (e. g., Wanner and Gujer 1986, Wanner and Reichert 1996, Tiwari and Bowers 2001, Lee and Park 2007), improved microscopic techniques in recent

decades have revealed a rich diversity of biofilm structure varying from smooth flat biofilm to forms described as towers, mushrooms, streamers, pores, and channels (e. g., Costerton 2007). Repeatability is notoriously challenging in biofilm experiments, but results (reviewed by Stoodley *et al.* 2002) broadly suggest that such architectural forms are favoured under scarce nutrient conditions and relatively low fluid flow. By contrast, high fluid flow and/or high nutrient conditions favour relatively flat biofilm.

The need to understand biofilm architecture stems from the interdependence of the surface architecture, transport of dissolved species (including nutrients, metabolites, disinfectants) across the biofilm/fluid interface, growth rate, and fluid flow. For a given surface density of biofilm biomass, the overall chemical exchange, biofilm permeability, flow resistance in confined flow paths, cell attachment/detachment and sloughing may all be presumed to depend on the surface architecture and may affect a range of practical applications. Detachment and sloughing further affect the spread of biofilm and clogging of downstream flow paths.

Many modelling studies of biofilm growth have used discrete approaches to describe the biomass, including cellular automata and individual-based models (reviewed by Lapidou *et al.* (2010), for example). These provide a useful means to perform simulations that readily allow consideration of complex scenarios such as multi-species biofilm, multi-component biochemistry and interactions with fluid flow. However, the physical properties of biofilm are dominated by the slime matrix rather than the cellular component, and in the interests of computational tractability these discrete biomass models take a simplified approach to mechanical deformation. The formation of surface architecture, in particular, depends on the manner in which growth-induced stresses are accommodated. A growing number of experimental studies aim to characterise the mechanical properties of biofilm (reviewed by Böl *et al.* (2013)), which behaves as a viscoelastic solid relaxing to a viscous fluid on times of the order of a minute. For a timescale relevant to biofilm growth (hours to days), a viscous fluid description is appropriate. There is therefore a distinct breed of continuum biofilm models which focus, somewhat more theoretically, on the mechanical description of the biofilm, and in particular the slime matrix. In contrast, Ben Amar and Wu (2014) present a model for the formation of biofilm pattern which relies on a characterisation of the biofilm as an elastic medium.

Dockery and Klapper (2002) used a simple Darcy flow model to describe growth of biofilm with a single substrate supplied across a fixed-width diffusive boundary layer. Their analysis of a 1D travelling wave solution, corresponding to uniform thick biofilm, revealed a fingering instability mechanism selecting surface structure at a wavelength equal to the length scale of substrate penetration into the biofilm.

More recently, several continuum models have been proposed based on polymer solution theory, to reflect the composition of the slime matrix as a solution largely of extracellular polymeric substances (EPS) in water. Polymer solutions differ from simple solutions in that the conformational entropy of polymer chains even in dilute solution can have significant impact on the rheology. For a solution with volume fraction  $\phi$  of polymer, Flory–Huggins theory (Flory 1953) provides the simplest theoretical description of a free energy of mixing governing the composition-dependent

tendency of a polymer solution to imbibe further solvent. In particular, the fact that biofilm tends not to swell indefinitely suggests the existence of a non-trivial equilibrium composition and is consistent with the ‘poor solvent’ régime of polymer solutions. An additional gradient free energy term (cf. Cahn and Hilliard (1958)) can become relevant in spatially inhomogeneous solutions and in describing the dynamics of phase separation, which has recently been suggested to have relevance to biofilm (Ghosh *et al.* 2015).

Cogan and Keener (2004) used a two-fluid model for the biofilm matrix, with an EPS polymer phase occupying only a small volume fraction  $\phi$  relative to the solvent water phase. They ignored the cellular component of biofilm, taking growth of the polymer phase as a proxy for bacterial growth. Both phases were modelled as Newtonian viscous fluids, and the difference between the phase-averaged pressures was constituted via an osmotic pressure term based on a Flory–Huggins-like free energy of mixing. The model was simplified by neglecting inertial terms and interphase drag (thereby decoupling the phases), and assuming a dominant balance between the EPS phase viscous stress and the osmotic pressure term. Analysing the stability of a 1-D travelling wave solution with specified nutrient concentration at the biofilm surface (rather than across a boundary layer as in Dockery and Klapper (2002)), they identified an instability mechanism with mode selection at a finite wavelength dependent on the strength of surface tension.

Zhang *et al.* (2008a,b) similarly ignored the cellular volume fraction and modelled biofilm as an EPS-water polymer solution. But rather than neglect the water phase velocity, they used a drift flux approach to the two phase flow, identifying a mixture velocity and an additional polymer network drift flux relative to the mixture. The drift flux was taken as proportional to the gradient of the osmotic pressure, in which they also included a Cahn–Hilliard-like gradient energy term. The model provided a framework for comparing various material models to constitute the EPS-water mixture stress state, including Newtonian viscous and Johnson–Segelman viscoelastic rheology. Results of steady state analysis for the various models suggest linear instability with a finite selected wavelength, consistent with results of earlier models (Picioareanu *et al.* 1998, Dockery and Klapper 2002, Cogan and Keener 2004). Numerical simulations and extensions of this model have provided the basis for subsequent studies such as those of Lindley *et al.* (2012) and Zhang (2012).

Seminara *et al.* (2012) performed experiments on wild-type and EPS- and flagella-deficient strains of *Bacillus subtilis*. Disc-shaped colonies on agar plates were modelled with a two-fluid polymer solution model assuming dominant momentum balance between osmotic pressure and EPS viscous stress. Further assumptions included swelling quasi-equilibrium (small variation in biofilm composition from swelling equilibrium) and a lubrication theory approximation to reduce the spatial dimension of the model based on the thin disc morphology of the observed biofilm colonies. The model reduced to a degenerate porous medium type equation for the radial biofilm depth variation, assuming a leading pre-wetted film rather than dealing explicitly with the contact line. The model supported the proposition that biofilm spread is controlled by swelling due to growth-generated osmotic pressure, rather than direct inter-neighbour cell jostling.

Winstanley *et al.* (2011) started from a two-fluid model with Newtonian viscous stresses, and used estimates of model parameters to argue that the viscous stress terms are in fact negligible: at time scales larger than minutes the dominant momentum balance is between interphase drag and osmotic pressure (contrary to the assumptions of Cogan and Keener (2004)). An estimate of the gradient energy parameter suggested that a sharp interface approximation is appropriate for model domains with spatial scale larger than a few microns. The study investigated 1-D solutions and outlined a potential simplification for the model in higher dimensions.

In this paper we elaborate on the reduction of the Winstanley *et al.* (2011) model in one lateral dimension in the simplifying régime where EPS concentration variation through the biofilm is small. We analyse the stability of one-dimensional solutions and show that numerical solutions are consistent with the stability results.

## 2 Biofilm model

We begin by recalling the polymer/solvent model presented by Winstanley *et al.* (2011). The EPS has volume fraction  $\phi$ , which is taken to include also the bacteria cells, which themselves produce the EPS. The phase-averaged velocity of the EPS is denoted  $\mathbf{v}$ , so that the EPS flux is  $\phi\mathbf{v}$ , and the conservation of EPS is described by the equation

$$\phi_t + \nabla \cdot (\phi\mathbf{v}) = \phi g(c). \quad (2.1)$$

Here  $g$  is a specific growth term, having units of one over time, and represents the net fractional volumetric rate of extrusion of EPS from the bacterial cells (as well as the growth of the cells themselves). While it may plausibly also depend on the EPS volume fraction, we assume it depends only on the concentration of a rate-limiting nutrient, which for example could be a terminal electron acceptor such as oxygen. Winstanley *et al.* proposed the commonly adopted Monod form:

$$g = \frac{Gc}{K + c}, \quad (2.2)$$

where  $c$  is the nutrient concentration, and  $G$  and  $K$  are constants.

In a similar manner, conservation of the water phase is described by

$$-\phi_t + \nabla \cdot [(1 - \phi)\mathbf{w}] = 0, \quad (2.3)$$

where  $\mathbf{w}$  is the phase-averaged water velocity. Uptake and transport of nutrient is given by

$$[(1 - \phi)c]_t + \nabla \cdot [(1 - \phi)c\mathbf{w}] = \nabla \cdot [(1 - \phi)D\nabla c] - \phi r(c); \quad (2.4)$$

the equation represents a conservation law for the concentration  $c$  of nutrient, allowing also for molecular diffusion, as well as the uptake of nutrient by the bacteria;  $D$  is the diffusion coefficient, and we take the uptake function to be

$$r = \frac{Rc}{K + c}, \quad (2.5)$$

so that  $G/R$  is a yield coefficient for the EPS growth.

The differential equations of the model are completed by a momentum equation for each phase:

$$\begin{aligned} \mathbf{0} &= \mu_{\text{EPS}} \nabla \cdot [\phi \mathbf{T}] - \frac{\mu_w}{k} (1 - \phi)^2 (\mathbf{v} - \mathbf{w}) - \nabla \Psi - \phi \nabla p, \\ \mathbf{0} &= \frac{\mu_w}{k} (1 - \phi)^2 (\mathbf{v} - \mathbf{w}) - (1 - \phi) \nabla p, \end{aligned} \quad (2.6)$$

where the tensor  $\mathbf{T}$  is

$$\mathbf{T} = \nabla \mathbf{v} + \nabla \mathbf{v}^T - \theta (\nabla \cdot \mathbf{v}) \boldsymbol{\delta} \quad (2.7)$$

(Batchelor 1967)<sup>1</sup>, where  $\boldsymbol{\delta}$  is the unit tensor,  $\mu_{\text{EPS}}$  and  $\mu_w$  are the viscosities of EPS and water, respectively,  $k$  is the medium permeability, and  $p$  is the fluid pressure. These equations are properly derived from models of slow, two-phase viscous flow (Drew and Passman 1999), in which the inertial terms are neglected, and there is an interactive drag between the phases, here chosen as a term proportional to the velocity difference, and such that the water momentum equation is equivalent to Darcy's law. Winstanley *et al.* additionally included a viscous term for the water, but showed that it was negligible and inconsequential, and so we omit it here.

In two-phase flow theory, the pressures of each phase are generally different and a relation between them must be prescribed, based on the microscale description of the media. In the present case, consideration of the Flory-Huggins theory of polymer interaction (Flory 1953) leads to a description of this relation in terms of an osmotic pressure  $\Psi$  which can be approximately given for small values of  $\phi$  by

$$\Psi \approx E_L \left[ - \left( \chi - \frac{1}{2} \right) \phi^2 + \frac{1}{3} \phi^3 \right], \quad (2.8)$$

where  $E_L$  is the monomer site energy density, and  $\chi$  is the Flory interaction parameter.<sup>2</sup> Evidently, (2.6)<sub>2</sub> allows us to define an EPS pressure of the form

$$p_s = p + \int_{\phi_{\text{eq}}}^{\phi} \frac{\Psi'(\phi) d\phi}{\phi}. \quad (2.9)$$

A stable equilibrium between the two-phase mixture and the pure solvent occurs when the osmotic pressure is zero and  $\Psi' > 0$ , and thus

$$\phi = \phi_{\text{eq}} = 3 \left( \chi - \frac{1}{2} \right). \quad (2.10)$$

The boundary conditions for the equations, suitable to describe a growing biofilm in  $0 < z < s(x, y, t)$ , where  $z$  is the distance from the wall at  $z = 0$  to which the

<sup>1</sup>The usual value of  $\theta = \frac{2}{3}$ . The divergence term in (2.7) was omitted by Winstanley *et al.* (2011), i. e.,  $\theta = 0$ . Inclusion of a bulk viscosity  $\mu_B$  (Batchelor 1967, p. 154) would give a value  $\theta = \frac{2}{3} - \mu_B/\mu_{\text{EPS}}$ . We will proceed with the general term  $\theta$ , though as we shall see, the precise value has little effect.

<sup>2</sup>The factor  $\frac{1}{3}$  was incorrectly given as  $\frac{1}{6}$  in equation (2.7) of Winstanley *et al.* (2011), with largely cosmetic consequences.

biofilm is attached, are those of no slip of EPS, no flow of water through the wall, and no flux of nutrient at the wall:

$$\mathbf{v} = \mathbf{0}, \quad \mathbf{w} \cdot \mathbf{n} = 0, \quad \frac{\partial p}{\partial n} = 0, \quad \frac{\partial c}{\partial n} = 0 \quad \text{at } z = 0; \quad (2.11)$$

at the top of the biofilm, suitable conditions are those of a prescribed concentration influx, prescribed  $\phi$  (specifically representing the stable equilibrium  $\Psi = 0$  where  $\Psi' > 0$ , if  $\chi > \frac{1}{2}$ , as we assume), continuous water pressure, and no traction on the EPS:

$$d_c \frac{\partial c}{\partial n} = c_0 - c, \quad \phi = 3(\chi - \frac{1}{2}), \quad p = 0, \quad \boldsymbol{\sigma} \cdot \mathbf{n} = \mathbf{0} \quad \text{at } z = s, \quad (2.12)$$

where  $d_c$  is a suitable mass transfer coefficient, representing the thickness of a boundary layer over which the external concentration varies; the stress tensor is

$$\boldsymbol{\sigma} = -p_s \boldsymbol{\delta} + \mu_{\text{EPS}} \mathbf{T}; \quad (2.13)$$

in addition there is a kinematic condition

$$s_t + \mathbf{v} \cdot \nabla (s - z) = 0, \quad (2.14)$$

which arises from the usual fluid mechanical assumption that particles on the interface remain there, or in other words, the velocity of the interface is equal to the velocity of particles on it. Winstanley *et al.* (2011) showed that these conditions are sufficient to fully determine the solution for the growth of a laterally uniform biofilm.

Note that this model shares a problem with one of an ordinary viscous fluid, which stems from the combination of the kinematic condition (2.14) and the no slip boundary condition in (2.11), which together imply that the margin of the biofilm patch is unable to move because the cells adhere to the wall. Rather than address this issue here, in this paper we consider the behaviour of a biofilm patch far from its margin. Fowler and Winstanley (2012) have developed a new theory, which they call *flux intensity theory*, to describe the motion near the margin, and a future piece of work will combine that with the current study.

## 2.1 Non-dimensionalisation

The model is non-dimensionalised in exactly the same way as in Winstanley *et al.* (2011). The dimensionless form of the model can be written as

$$\begin{aligned} \phi_t + \nabla \cdot (\phi \mathbf{v}) &= \phi g, \quad g = \frac{c}{\kappa + c}, \\ -\varepsilon \phi_t + \nabla \cdot [(1 - \varepsilon \phi) \mathbf{w}] &= 0, \\ \alpha(1 - \varepsilon \phi)[c_t + \mathbf{w} \cdot \nabla c] &= \nabla \cdot [(1 - \varepsilon \phi) \nabla c] - \phi g, \\ \mathbf{0} &= \beta \nabla \cdot [\phi \mathbf{T}] - \phi(1 - \varepsilon \phi)(\mathbf{v} - \mathbf{w}) - \nabla \Psi - \varepsilon \phi \nabla p, \\ \mathbf{0} &= \beta \nabla \cdot [\phi \mathbf{T}] - \nabla \Psi - \nabla p, \\ \mathbf{T} &= \nabla \mathbf{v} + \nabla \mathbf{v}^T - \theta(\nabla \cdot \mathbf{v}) \boldsymbol{\delta}, \\ \Psi &= -\lambda \phi^2 + \frac{1}{3} \phi^3 + O(\varepsilon), \end{aligned} \quad (2.15)$$

Symbol	Typical value
$\alpha$	$1.37 \times 10^{-4}$
$\beta$	$1.1 \times 10^{-4}$
$\eta$	$O(1)$
$\varepsilon$	$0.37 \times 10^{-2}$
$\kappa$	0.35
$\lambda$	$O(1)$

Table 1: Typical values of the dimensionless parameters. The values of  $\eta$  and  $\lambda$  are not well constrained.

and the dimensionless parameters are identical to those in the earlier paper. The parameter  $\lambda$  can be defined (taking into account the footnote following (2.8)) as  $\lambda = \phi_{\text{eq}}/3\phi_0$ , where  $\phi_0$  is the scale used for the volume fraction of EPS, and is determined by a balance between the osmotic pressure and the interfacial drag, while  $\phi_{\text{eq}}$  is the equilibrium fraction of EPS, typically 1–5%; Winstanley (2011, p. 66) estimated typical values  $\lambda = 0.9\text{--}4.5$  (the values 0.5–2.3 of Winstanley *et al.* (2011) are associated with the incorrect factor  $\frac{1}{6}$  which they used in (2.8) above).

### Boundary conditions

The scaled boundary conditions take the form

$$\mathbf{v} = \mathbf{0}, \quad \mathbf{w} \cdot \mathbf{n} = 0, \quad \frac{\partial p}{\partial z} = \frac{\partial c}{\partial z} = 0 \quad \text{on} \quad z = 0, \quad (2.16)$$

and

$$\eta \frac{\partial c}{\partial n} = 1 - c, \quad p = 0, \quad \boldsymbol{\sigma} \cdot \mathbf{n} = \mathbf{0}, \quad \phi = 3\lambda \quad \text{on} \quad z = s, \quad (2.17)$$

where the scaled stress tensor is

$$\boldsymbol{\sigma} = -p_s \boldsymbol{\delta} + \frac{\beta \mathbf{T}}{\varepsilon}, \quad (2.18)$$

and

$$p_s = p + \frac{1}{\varepsilon} \int_{3\lambda}^{\phi} \frac{\Psi'(\phi) d\phi}{\phi}. \quad (2.19)$$

The parameter  $\eta$  is defined by

$$\eta = \frac{d_c}{d}, \quad (2.20)$$

where the length scale  $d$  is of the order of a typical biofilm thickness,  $d \sim 100 \mu\text{m}$ .

Lastly the kinematic boundary condition on  $z = s$  takes the form

$$s_t + \mathbf{v} \cdot \nabla (s - z) = 0. \quad (2.21)$$

Estimates of the parameters as described by Winstanley *et al.* (2011) are given in table 1. The parameter  $\eta$  was not used by them, as they assumed prescribed concentration  $c$  at the free surface, equivalently  $\eta = 0$ . Taking  $\eta > 0$  allows for finite nutrient transfer rate from the medium above.

## 2.2 Reduction of the model

The parameters  $\alpha$ ,  $\beta$  and  $\varepsilon$  are all small, and we will eventually consign them all towards zero. Putting  $\alpha = 0$  is an assumption of quasi-static reaction kinetics which is commonly made (Klapper 2012), the basis of which is lucidly discussed by Kissel *et al.* (1984). The asymptotic procedure which we use is novel and non-standard. The neglect of  $\beta$  is a singular perturbation, for which the normal procedure would be to additionally neglect an associated boundary condition associated with boundary layer behaviour. While we do this, the reduced model obtained is degenerate, and some subtlety is required in elucidating the correct behaviour.

Before beginning our asymptotic simplification, we rescale the equations based on Winstanley *et al.*'s observation that even for moderate  $\lambda$ , the assumption of large  $\lambda$  is highly accurate. This suggests that we first rescale the model using

$$\phi = 3\lambda(1 + \nu\Phi), \quad s, \mathbf{x}, \mathbf{v}, \mathbf{w} \sim \frac{1}{\sqrt{3\lambda}}, \quad (2.22)$$

where

$$\nu = \frac{1}{9\lambda^3}. \quad (2.23)$$

This leads to the model equations in the form

$$\begin{aligned} \nu\Phi_t + \nabla \cdot [(1 + \nu\Phi)\mathbf{v}] &= (1 + \nu\Phi)g, \\ -3\lambda\varepsilon\nu\Phi_t + \nabla \cdot [\{1 - 3\lambda\varepsilon(1 + \nu\Phi)\}\mathbf{w}] &= 0, \\ \frac{\alpha}{3\lambda}\{1 - 3\lambda\varepsilon(1 + \nu\Phi)\}[c_t + \mathbf{w} \cdot \nabla c] &= \nabla \cdot [\{1 - 3\lambda\varepsilon(1 + \nu\Phi)\}\nabla c] - (1 + \nu\Phi)g, \\ \mathbf{0} &= 3\lambda\beta\nabla \cdot [(1 + \nu\Phi)\mathbf{T}] - (1 + \nu\Phi)[1 - 3\lambda\varepsilon(1 + \nu\Phi)](\mathbf{v} - \mathbf{w}) \\ &\quad - \nabla\Psi - 3\lambda\varepsilon(1 + \nu\Phi)\nabla p, \\ \mathbf{0} &= 3\lambda\beta\nabla \cdot [(1 + \nu\Phi)\mathbf{T}] - \nabla\Psi - \nabla p, \\ \mathbf{T} &= \nabla\mathbf{v} + \nabla\mathbf{v}^T - \theta(\nabla \cdot \mathbf{v})\boldsymbol{\delta}, \\ \Psi &= \Phi + O(\nu). \end{aligned} \quad (2.24)$$

The boundary conditions take the same form as before, except that now

$$\frac{\partial\Phi}{\partial z} = 0 \text{ on } z = 0, \quad \Phi = 0 \text{ on } z = s, \quad (2.25)$$

the scaled EPS pressure is

$$p_s = p + \frac{1}{3\varepsilon\lambda}[\Phi + O(\nu)]. \quad (2.26)$$

A notional estimate is  $3\lambda \approx 10$ , and thus we suppose that the terms in  $\alpha$  and  $\varepsilon$  are negligible in (2.24), but we temporarily retain the terms in  $\beta$ . Additionally we suppose that  $\nu \ll 1$ , which requires only that  $\lambda \gtrsim 1$ . For convenience we define

$$\bar{\beta} = 3\lambda\beta \sim 10^{-3}. \quad (2.27)$$

Ignoring the terms in  $\alpha$ ,  $\varepsilon$  and  $\nu$ , the equations can now be written in the form

$$\begin{aligned}
\nabla \cdot \mathbf{v} &= g, & g &= \frac{c}{\kappa + c}, \\
\nabla \cdot \mathbf{w} &= 0, \\
\nabla^2 c &= g, \\
\mathbf{v} - \mathbf{w} &= \nabla p, \\
\bar{\beta} \nabla \cdot \mathbf{T} &= \bar{\beta} [\nabla^2 \mathbf{v} + (1 - \theta) \nabla (\nabla \cdot \mathbf{v})] = \nabla \Phi + \nabla p, \\
\mathbf{T} &= \nabla \mathbf{v} + \nabla \mathbf{v}^T - \theta (\nabla \cdot \mathbf{v}) \boldsymbol{\delta};
\end{aligned} \tag{2.28}$$

the upper stress boundary condition is, from (2.17), (2.18), (2.26) and (2.27), allowing for the fact that  $p = \Phi = 0$  at  $z = s$ ,

$$\mathbf{T} \cdot \mathbf{n} = (\nabla \mathbf{v} + \nabla \mathbf{v}^T) \cdot \mathbf{n} - \theta (\nabla \cdot \mathbf{v}) \mathbf{n} = \mathbf{0}, \tag{2.29}$$

and the kinematic condition is

$$s_t + \mathbf{v} \cdot \nabla (s - z) = 0. \tag{2.30}$$

Our earlier comments on the subtlety of the procedure are now evident in (2.28). If we simply put  $\bar{\beta} = 0$ , then we can solve for  $\mathbf{v} - \mathbf{w}$ , but not for the velocities individually. The problem is that (2.28)<sub>5</sub> implies that

$$\nabla \times [\nabla^2 \mathbf{v} + (1 - \theta) \nabla (\nabla \cdot \mathbf{v})] = 0, \tag{2.31}$$

but this extra constraint is lost if one immediately puts  $\bar{\beta} = 0$ . A little sleight of hand is therefore necessary to allow the limit  $\bar{\beta} \rightarrow 0$ . First, we define a function  $H$  via

$$\Phi + p = \bar{\beta} [H - \nabla^2 \Phi + (1 - \theta) \nabla \cdot \mathbf{v}]; \tag{2.32}$$

substituting this into (2.28)<sub>5</sub> then yields, using also (2.28)<sub>4</sub>, and without approximation,

$$\nabla H = \nabla^2 \mathbf{w} + \bar{\beta} \nabla^2 [\nabla^2 \mathbf{v} + (1 - \theta) \nabla (\nabla \cdot \mathbf{v})]. \tag{2.33}$$

If we now ignore the term in  $\bar{\beta}$ , we have the equations of Stokes flow for  $\mathbf{w}$ :

$$\begin{aligned}
\nabla \cdot \mathbf{w} &= 0, \\
\nabla H &= \nabla^2 \mathbf{w},
\end{aligned} \tag{2.34}$$

where the first equation is simply (2.28)<sub>2</sub>.

Equations (2.28)<sub>4</sub> and (2.28)<sub>5</sub> combine to yield

$$\mathbf{v} \approx \mathbf{w} - \nabla \Phi, \tag{2.35}$$

and then (2.28)<sub>1</sub>, (2.28)<sub>2</sub>, again neglecting the  $O(\bar{\beta})$  term, imply

$$-\nabla^2 \Phi \approx \nabla \cdot \mathbf{v} = g. \tag{2.36}$$

Because of the loss of the viscous terms in (2.28)<sub>5</sub>, it is possible that some of the boundary conditions on  $\mathbf{v}$ , and consequently  $\mathbf{w}$ , may not be satisfied. Boundary conditions for  $\mathbf{w}$  at  $z = 0$  follow from those of no slip for  $\mathbf{v}$ , and are

$$\mathbf{w} \cdot \mathbf{n} = 0, \quad \mathbf{w} \cdot \mathbf{t} = \nabla \Phi \cdot \mathbf{t} \quad \text{on } z = 0, \quad (2.37)$$

where  $\mathbf{t}$  is the tangent vector to the plane. Boundary conditions at the surface follow from the the normal stress condition (2.29) on  $\mathbf{v}$ , and this leads to

$$\mathbf{n} \cdot (\nabla \mathbf{w} + \nabla \mathbf{w}^T) = 2\mathbf{n} \cdot \nabla \nabla \Phi + \theta g \mathbf{n}. \quad (2.38)$$

This seems fine, in the sense that (2.37) and (2.38) provide two conditions each for the fourth order Stokes flow model (2.34), but they are non-standard in the sense that there is no condition on the pseudo-pressure  $H$ , which is suspicious. In fact, the constraint that  $\Phi = p = 0$  at  $z = s$ , together with (2.36), implies that

$$H = -(2 - \theta)g(c) \quad \text{on } z = s, \quad (2.39)$$

which together with (2.38) provides a further condition (thus one too many) for (2.34).

The resolution appears to lie in the fact that the neglect of  $\bar{\beta}$  in (2.28) is indeed singular, and there is a singular layer in which the viscous term is important. We combine (2.28)<sub>4</sub> and (2.28)<sub>5</sub> in the form

$$\bar{\beta}[\nabla^2 \mathbf{v} + (1 - \theta)\nabla(\nabla \cdot \mathbf{v})] = \mathbf{v} - (\mathbf{w} - \nabla \Phi). \quad (2.40)$$

Taking the normal component and denoting  $\mathbf{v} \cdot \mathbf{n} = v_n$ , the relevant boundary layer approximation of this is

$$\bar{\beta} \frac{\partial^2 v_n}{\partial n^2} = v_n - \left( w_n - \frac{\partial \Phi}{\partial n} \right), \quad (2.41)$$

where  $\frac{\partial}{\partial n} = \mathbf{n} \cdot \nabla$ , and the second term on the left remains small since  $\nabla \cdot \mathbf{v} = g$ , and thus its normal component is  $\bar{\beta} g'(c) \frac{\partial c}{\partial n}$ , which is small as  $c$  has no singular behaviour; the approximate solution of (2.41) satisfying the normal component of (2.29), which is

$$\frac{\partial v_n}{\partial n} = \frac{1}{2} \theta g, \quad (2.42)$$

and decaying far from the boundary is

$$v_n = \left( w_n - \frac{\partial \Phi}{\partial n} \right) + \frac{1}{2} \theta \sqrt{\bar{\beta}} g \exp \left[ \frac{n}{\sqrt{\bar{\beta}}} \right], \quad (2.43)$$

where  $n = |\mathbf{n}|$ , and we take  $\mathbf{n}$  pointing out of the biofilm patch. Thus the normal component of (2.29) is satisfied by means of a boundary layer, and it is not necessary that the outer solution satisfy this condition. The boundary conditions for (2.34) at the surface therefore consist of (2.39), together with the tangential component of (2.38), which takes the form, written in terms of components,

$$t_i n_j \left( \frac{\partial w_i}{\partial x_j} + \frac{\partial w_j}{\partial x_i} \right) = 2 t_i n_j \frac{\partial^2 \Phi}{\partial x_i \partial x_j}. \quad (2.44)$$

## Summary

$c$  and  $\Phi$  are determined by the equations

$$\begin{aligned} \nabla^2 c &= -\nabla^2 \Phi = g(c), & g(c) &= \frac{c}{\kappa + c}, \\ \eta \frac{\partial c}{\partial n} &= 1 - c, & \Phi &= 0 \quad \text{at } z = s, \\ \frac{\partial c}{\partial z} &= \frac{\partial \Phi}{\partial z} = 0 & & \text{at } z = 0. \end{aligned} \quad (2.45)$$

The cell velocity is then determined from

$$\mathbf{v} = \mathbf{w} - \nabla \Phi, \quad (2.46)$$

and the solvent velocity is determined by solution of the Stokes flow problem

$$\begin{aligned} \nabla \cdot \mathbf{w} &= 0, \\ \nabla H &= \nabla^2 \mathbf{w}, \end{aligned} \quad (2.47)$$

with the boundary conditions

$$\begin{aligned} w_n &= 0, & \mathbf{t} \cdot \mathbf{w} &= \mathbf{t} \cdot \nabla \Phi \quad \text{at } z = 0, \\ H &= -(2 - \theta)g(c), & t_i n_j \left( \frac{\partial w_i}{\partial x_j} + \frac{\partial w_j}{\partial x_i} \right) &= 2t_i n_j \frac{\partial^2 \Phi}{\partial x_i \partial x_j} \quad \text{at } z = s, \end{aligned} \quad (2.48)$$

Finally, the kinematic condition at the biofilm surface is simply

$$s_t + (\mathbf{w} - \nabla \Phi) \cdot \nabla (s - z) = 0. \quad (2.49)$$

## 3 Stability

### 3.1 One-dimensional solution

Winstanley *et al.* (2011) gave a one-dimensional solution of the above system in the case that  $\eta = 0$ , though with only tangential discussion of the limit  $\nu \rightarrow 0$ . If solutions depend only on  $z$  and  $t$ , then we find  $H$  is constant,  $\mathbf{w} = \mathbf{0}$ , and the model reduces to

$$\begin{aligned} \Phi &= c_s - c, & \dot{s} &= c'_s, \\ c'' &= \frac{c}{\kappa + c}, & c'(0) &= 0, & \eta c'_s &= 1 - c_s, \end{aligned} \quad (3.1)$$

where  $c_s = c(s, t)$ ,  $c'_s = c_z(s, t)$ , the overdot denotes a time derivative and the prime denotes a spatial derivative with respect to  $z$ . The solution for  $c$  is a quadrature,

$$\int_{c_w}^c \frac{dc}{[A(c) - A(c_0)]^{1/2}} = z, \quad (3.2)$$

where we can take

$$A(c) = 2 \int_0^c g(c') dc' = 2 \left[ c - \kappa \ln \left( 1 + \frac{c}{\kappa} \right) \right] \quad (3.3)$$

(thus  $A(0) = 0$ ), and the basal concentration at the wall,  $c_w$ , is determined by

$$\int_{c_w}^{c_s} \frac{dc}{[A(c) - A(c_0)]^{1/2}} = s, \quad (3.4)$$

while the surface boundary condition for  $c$  gives

$$\eta \{A(c_s) - A(c_w)\}^{1/2} = 1 - c_s, \quad (3.5)$$

and  $s$  then satisfies the ordinary differential equation

$$\dot{s} = \{A(c_s) - A(c_w)\}^{1/2}. \quad (3.6)$$

This solution settles, as  $t \rightarrow \infty$  for finite  $\kappa$ , to a travelling wave solution in which  $c_w \rightarrow 0$ ,  $\dot{s} \rightarrow V = \sqrt{A(c_s)} = \sqrt{2 - 2\kappa \ln \left( 1 + \frac{1}{\kappa} \right)}$ , and  $c$  is given implicitly by

$$z - s = z - Vt = - \int_c^{c_s} \frac{dc}{\sqrt{A(c)}}, \quad (3.7)$$

and  $c_s$  is given by

$$\eta \sqrt{A(c_s)} = 1 - c_s. \quad (3.8)$$

### 3.2 Linear stability analysis

We study the stability of the travelling wave solution given above. We assume a two-dimensional flow in which the coordinates are  $x, z$ , and we can then define a stream function  $\psi$  such that

$$\mathbf{w} = (\psi_z, -\psi_x). \quad (3.9)$$

The normal and tangent vectors are

$$\mathbf{n} = \frac{(-s_x, 1)}{(1 + s_x^2)^{1/2}}, \quad \mathbf{t} = \frac{(1, s_x)}{(1 + s_x^2)^{1/2}}, \quad (3.10)$$

and then the boundary conditions at the surface take the form

$$\begin{aligned} (1 - s_x^2)(\psi_{zz} - \psi_{xx} - 2\Phi_{xz}) &= 2s_x(\Phi_{zz} - \Phi_{xx} + 2\psi_{xz}), \\ H &= -(2 - \theta)g(c), \quad \Phi = 0, \\ \frac{\eta(c_z - s_x c_x)}{(1 + s_x^2)^{1/2}} &= 1 - c, \\ s_t + \psi_x + \Phi_z + (\psi_z - \Phi_x)s_x &= 0, \end{aligned} \quad (3.11)$$

while the boundary conditions at the base become

$$c, \psi \rightarrow 0, \quad \Phi \rightarrow c_s \quad \text{as} \quad z \rightarrow -\infty, \quad (3.12)$$

where  $c_s$  is the constant solution of (3.8).

We change to a moving frame in which

$$s = Vt + \Sigma, \quad z = Vt + \zeta; \quad (3.13)$$

other than changing  $z$  to  $\zeta$  and  $s$  to  $\Sigma$  in the equations and boundary conditions, the only change occurs in the kinematic condition, which becomes

$$V + \Phi_\zeta + \Sigma_t + \psi_x + (\psi_\zeta - \Phi_x)\Sigma_x = 0 \quad \text{on} \quad \zeta = \Sigma. \quad (3.14)$$

The basic state for the system is

$$\begin{aligned} \psi &= 0, \quad \Sigma = 0, \quad \Phi_0 = c_s - c, \\ H &= -(2 - \theta)g(c_s), \quad \sqrt{A(c_s)} = \frac{1 - c_s}{\eta} = V, \\ c &= c_0(\zeta), \quad \zeta = - \int_c^{c_s} \frac{dc'}{\sqrt{A(c')}}. \end{aligned} \quad (3.15)$$

Denoting perturbations to  $\psi, c, \Phi, H$  by  $\Psi, C, \phi, h$  respectively, we find the linearised equations are

$$\begin{aligned} h_x &= \nabla^2 \Psi_\zeta, \\ h_\zeta &= -\nabla^2 \Psi_x, \\ \nabla^2 C &= -\nabla^2 \phi = g'(c_0)C, \end{aligned} \quad (3.16)$$

with linearised boundary conditions

$$C, \Psi, \phi \rightarrow 0 \quad \text{as} \quad \zeta \rightarrow -\infty \quad (3.17)$$

and

$$\begin{aligned} \phi_\zeta + \Phi_0''\Sigma + \Sigma_t + \Psi_x &= 0, \\ \Psi_{\zeta\zeta} - \Psi_{xx} - 2\phi_{x\zeta} &= 2\Phi_0''\Sigma_x, \\ h &= -(2 - \theta)g'(c_s)(C + c_0'\Sigma), \\ \phi + \Phi_0'\Sigma &= 0, \\ -(C + c_0'\Sigma) &= \eta(C_\zeta + c_0''\Sigma) \quad \text{on} \quad \zeta = 0. \end{aligned} \quad (3.18)$$

We take

$$\Sigma = e^{ikx + \sigma t}, \quad k > 0, \quad (3.19)$$

without loss of generality, and then

$$\Psi = f(\zeta)\Sigma, \quad C = b(\zeta)\Sigma, \quad \phi = a(\zeta)\Sigma, \quad h = d(\zeta)\Sigma, \quad (3.20)$$

where we find

$$\begin{aligned} f &= (A + B\zeta)e^{k\zeta}, \quad d = -2iBke^{k\zeta}, \\ a &= De^{k\zeta} - b(\zeta), \\ b'' &= [k^2 + g'\{c_0(\zeta)\}]b, \end{aligned} \quad (3.21)$$

and the boundary conditions (3.18) then imply

$$\begin{aligned} \sigma &= -a'_0 - \Phi''_0 - ikA, \\ 2Bk + 2Ak^2 - 2ik(kD - b'_0) &= 2ik\Phi''_0, \\ ikB &= (1 - \frac{1}{2}\theta)g'_0(b_0 + c'_0), \\ D - b_0 + \Phi'_0 &= 0, \\ b_0 + c'_0 &= -\eta(b'_0 + g_0), \end{aligned} \quad (3.22)$$

where  $a'_0 = a'(0)$ ,  $b_0 = b(0)$ ,  $b'_0 = b'(0)$ , and the other quantities with suffix zero are steady state solutions evaluated at  $\zeta = 0$ .

Simplification of this yields

$$\sigma = \frac{(1 - \frac{1}{2}\theta)(b_0 + c'_0)g'_0}{k}, \quad (3.23)$$

and the value of  $b_0$  is determined from the boundary value problem

$$\begin{aligned} b'' &= [k^2 + g'\{c_0(\zeta)\}]b, \\ \eta b' + b &= -\eta g_0 - c'_0 \quad \text{at } \zeta = 0, \\ b &\rightarrow 0 \quad \text{as } \zeta \rightarrow -\infty. \end{aligned} \quad (3.24)$$

To assess the stability criterion (3.23), we take as a non-restrictive example the function

$$g(c) = \mu c, \quad (3.25)$$

then the equation for  $b$  (and  $c_0$ ) can be solved, giving

$$c_0 = \frac{e^{\sqrt{\mu}\zeta}}{1 + \eta\sqrt{\mu}}, \quad b = -\frac{\sqrt{\mu}e^{(k^2 + \mu)^{1/2}\zeta}}{1 + \eta(k^2 + \mu)^{1/2}}, \quad (3.26)$$

from which we find

$$\sigma = \frac{(1 - \frac{1}{2}\theta)\mu^{3/2}\eta[(k^2 + \mu)^{1/2} - \sqrt{\mu}]}{[1 + \eta(k^2 + \mu)^{1/2}][1 + \eta\sqrt{\mu}]k}, \quad (3.27)$$

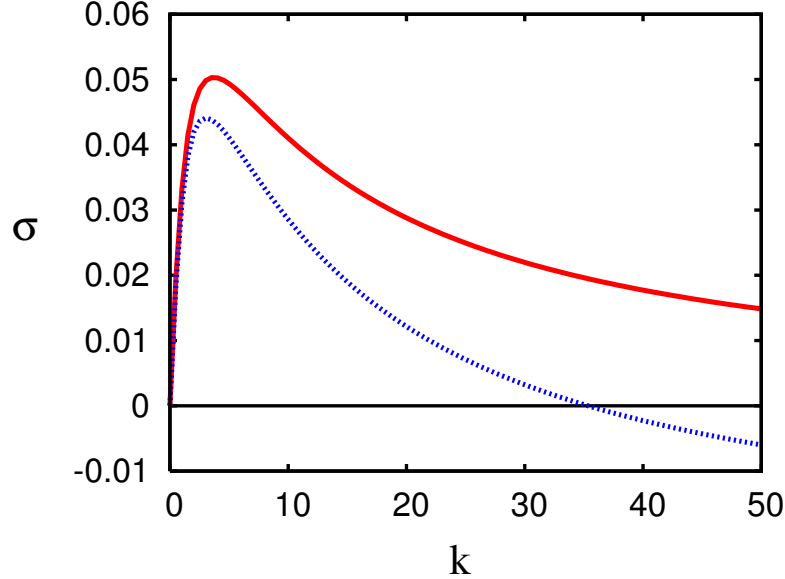


Figure 1: The growth rate  $\sigma$  as a function of wavenumber  $k$ , using (3.30) with parameters  $\mu = 1$ ,  $\eta = 0.1$ ,  $\theta = 0$ . The full line gives the rate for  $\bar{\beta} = 0$ , the dashed one for  $\bar{\beta} = 0.005$ .

which is positive, since we may take  $\theta \leq \frac{2}{3}$ . Note that when  $\eta = 0$ ,  $\sigma = 0$ , and the steady state is neutrally stable. For  $\eta \neq 0$ , the growth rate tends to zero as  $k \rightarrow 0$  and  $k \rightarrow \infty$ , and apparently the model is missing some dissipative term which would enable stabilisation at high wave number.

In more detail, we may illustrate the situation with the toy system

$$\begin{aligned} u_{xx} &= u - v, \\ v_t &= u + Dv_{xx}, \end{aligned} \tag{3.28}$$

for which perturbations to the steady state  $u = v = 0$  have solutions  $\propto \exp(\sigma t + ikx)$ , where

$$\sigma = \frac{1}{1 + k^2} - Dk^2. \tag{3.29}$$

The solution is linearly unstable at long wavelengths (small  $k$ ), but the diffusion term causes  $\sigma$  to become negative at large  $k$ , and the solution is well posed. However, if  $D = 0$ , the second equation becomes hyperbolic, and  $\sigma \rightarrow 0$  as  $k \rightarrow \infty$ .

We suggest that the same sort of behaviour may be occurring here. In fact, it seems the remaining dissipative term  $\propto \bar{\beta}$  in (2.28) may provide the required stabilising term. A partial argument for this can be given by re-doing the stability analysis above by replacing (2.47)<sub>2</sub> with (2.33). Following the same analysis through, we find that (3.27) is replaced by

$$\sigma = \frac{\mu^{3/2}}{\{1 + \eta(k^2 + \mu)^{1/2}\}} \left[ \frac{(1 - \frac{1}{2}\theta)\eta\{(k^2 + \mu)^{1/2} - \sqrt{\mu}\}}{(1 + \eta\sqrt{\mu})k} - \frac{1}{2}\bar{\beta}\{1 + (1 - \theta)\mu\}k \right], \tag{3.30}$$

so that the weak viscous term provides a stabilising effect at large wavenumber. Illustration of the growth rate as a function of  $k$  is given in figure 1, both with and without the stabilising term. Note how small the growth rate is.

## 4 Numerical solutions

Despite the comments in the preceding section, we have not attempted to solve the model where the weak viscous terms are included. Instead we solve (2.45)–(2.47) using a front-fixing transformation (e. g., Crank, 1984), but to compare with the stability analysis we have used both the function  $g(c) = \frac{c}{c + \kappa}$  and the simpler  $g(c) = \mu c$ ; the results are similar, but we use the latter in our figures below. For our computations, we ignore the divergence term by putting  $\theta = 0$ . It can be shown that non-zero values of  $\theta$  lead to the same results, adjusted by a rescaling of the variables. This might

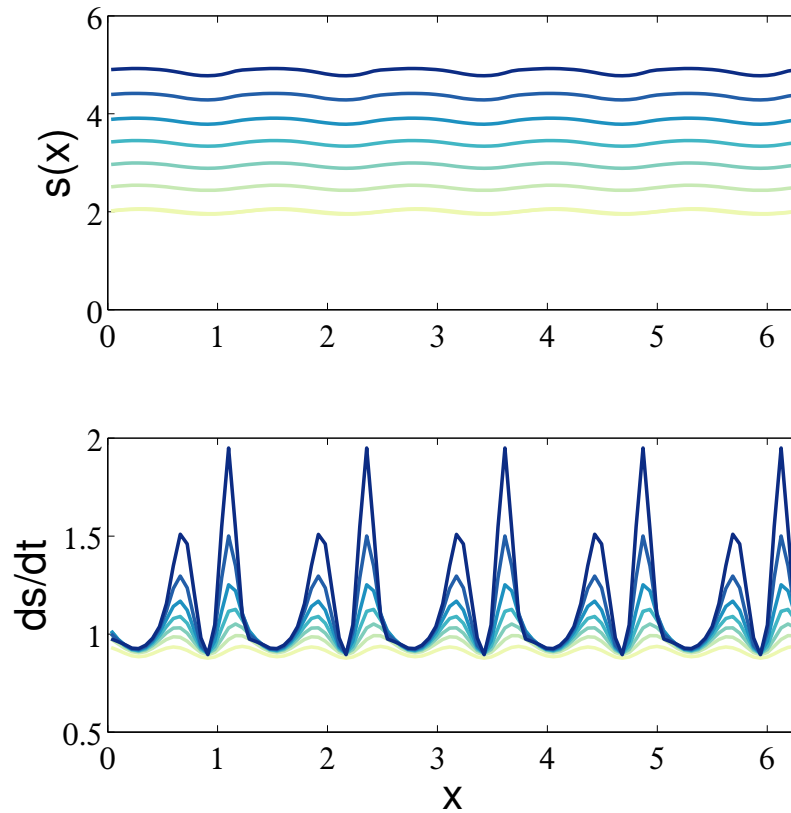


Figure 2: Evolution of the interface  $s$  at increasing times  $t = 0, 0.5, \dots, 3$  on a periodic domain of length  $2\pi$ , where the initial condition for  $s$  is  $s = 2 + 0.05 \sin 5x$ , and we have used  $g = \mu c$ , with the parameter values being  $\mu = 1$ ,  $\eta = 0.1$ . The top figure shows the growth of an instability, but it is more graphically realised by the lower figure showing  $s_t$ . This figure shows that the initial instability grows at double the spatial period, before evolving non-linearly towards a blow-up.

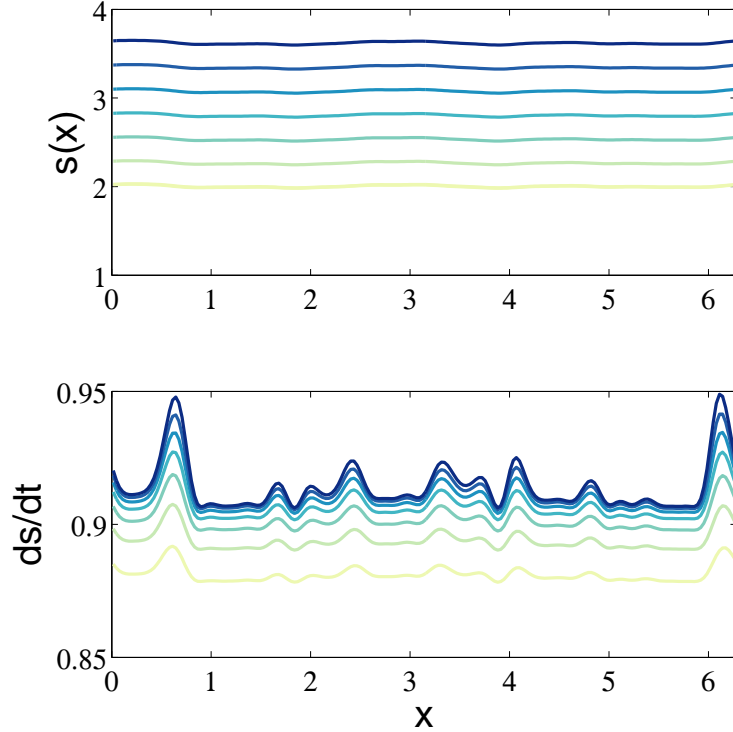


Figure 3: Evolution of the interface  $s$  at increasing times  $t = 0, 0.2, \dots, 1.2$  on a periodic domain of length  $2\pi$ , where the initial condition for  $s$  is  $s = 2 + 0.01\{\cos 2x + \sin 3x + 0.7 \cos 4x + 0.4 \sin 5x + 0.5 \sin 6x + 0.2 \cos 12x\}$ , and we have used  $g = \mu c$ , with the parameter values being  $\mu = 1$ ,  $\eta = 0.1$ . As explained in the text, this shows the development of localised instability from an irregular initial state.

also be inferred from (3.27). The problem is mapped from a domain with a time-dependent boundary to one with a fixed, time-independent boundary. This is done by a transformation of the vertical coordinate system from  $z$  to  $\xi$ , via  $\xi = z/s(x, t)$ . There are additional terms in the differential equations as a result, however we are able to implement a standard finite-difference scheme on a fixed grid after the transformation has been made.

After the coordinate transformation has been performed we discretise the governing equations and boundary conditions using a finite-difference scheme with semi-implicit time-stepping. We use a staggered, Cartesian, two-dimensional (2-D) grid with  $n_i \times n_j$  discrete points. There are periodic boundary conditions in  $x$  and boundary conditions (2.48)–(2.49) at the base and free surface. The nonlinear system of equations is solved using a Newton-Krylov solver, provided by the Portable Extensible Toolkit for Scientific Computation (Balay *et al.* 1997, 2013, 2014). At each time-step we solve for  $c$  and  $\phi$  via (2.45), before using these solutions in the boundary conditions for the coupled  $u, w$  and  $H$  solve. The solver finally uses explicit time stepping to

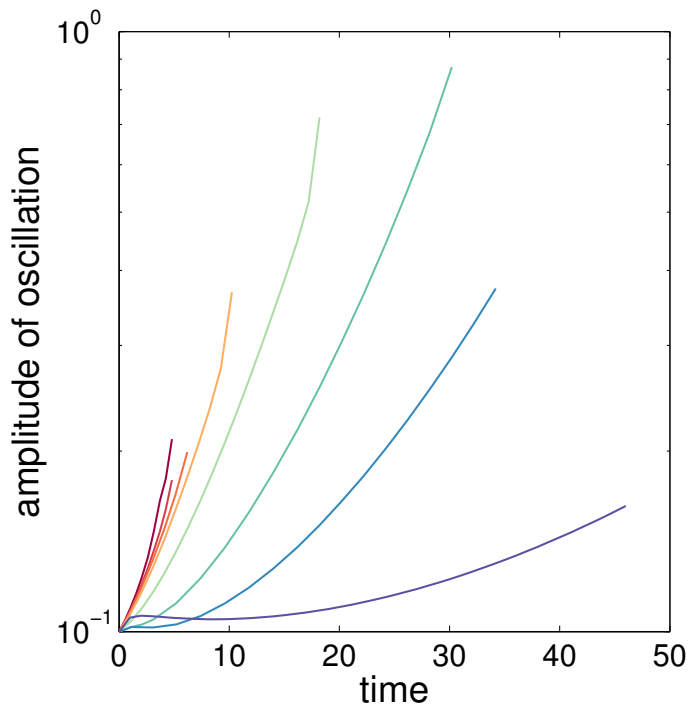


Figure 4: Evolution of the amplitude  $A$  of the spatial oscillation of  $s$  with time, for varying initial oscillation periods (and with periodic boundary conditions on the corresponding periodic domain). The function  $g$  is taken to be  $g = \mu c$ , with  $\mu = 1$ , and also  $\eta = 0.1$ . The wavenumbers of the initial perturbations are given by  $k = 2\pi/50 \approx 0.13$ ,  $2\pi/20 \approx 0.31$ ,  $2\pi/12 \approx 0.52$ , 1, 2, 3, 4, 5, in order of increasing eventual slope of the amplitude curves. For the first three curves, the domain lengths are 50, 20, 12 respectively, while for the last five they are all  $2\pi$ . Commentary on the choice of ‘the’ growth rate is given in the text.

solve for the new surface elevation. The solution at each step is accepted when the absolute size of the nonlinear system residual is less than  $10^{-8}$ .

We solve the system in domains of varying widths, all of sufficient depth that the travelling wave limit is an accurate description with  $c \rightarrow 1$  at the bed. To test stability of the system we introduce a perturbation to the initially flat surface. We do this with a regular perturbation in the form of a sine wave. The results are discussed in the following section.

As we shall see, while our numerical method is successful, the front-fixing method will break down when the the interface develops corners, which it does, due possibly to the neglect of the small viscous term in (2.33). One could of course simply include the viscous term, but realistic values of  $\bar{\beta}$  would then yield an impossibly stiff problem. The question then arises whether other methods might avoid this difficulty. Different numerical methods for this problem have been discussed by Du *et al.* (2013). Specifically, they develop an interface capturing method where the interface separates a viscous two-phase gel network and a viscous pure solvent. Their method uses an

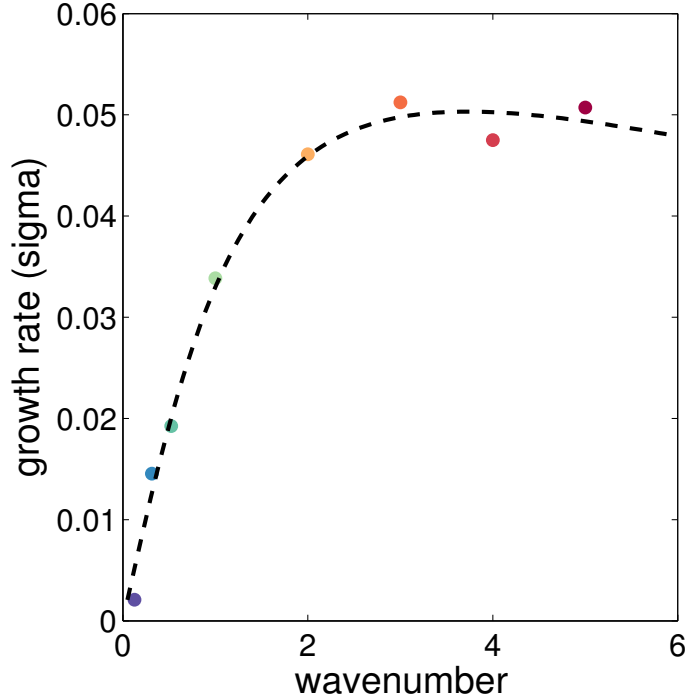


Figure 5: Growth rate determined from the numerical solution as portrayed in figure 4, compared with the theoretical result in (3.27). The parameters used were  $\mu = 1$  and  $\eta = 0.1$ . The same wave numbers are indicated as in figure 4, and the corresponding growth rates are determined as  $\sigma = \dot{A}/A$ , where  $A$  is the amplitude portrayed in figure 4, and the slopes are estimated from the curves between the time values 12 and 22 ( $k = 0.13$ ), 4 and 12 ( $k = 0.31$ ), 3 and 8 ( $k = 0.52, 1$ ), 3 and 7 ( $k = 2$ ), 2 and 7 ( $k = 3, 4$ ), and 2 and 6 ( $k = 5$ ). The reason for this is explained at the end of section 5, and is due to the fact that the curves in figure 4 do not indicate uniform exponential growth, but rather an initial relaxation phase, a subsequent exponential phase, and a final blow-up phase; the time intervals are chosen to select the exponential growth phase as well as possible.

artificial small additional network volume fraction  $\varepsilon$  in the equations, so that they solve the two-fluid viscous model everywhere, and the interface is ‘captured’ by the condition that the volume fraction reaches zero. With this addition, their numerical method then uses finite differences.

It seems that all such methods using finite differences will come to grief when the interface develops corners, and that a much more subtle approach would be necessary in order to track a non-smooth interface.

## 5 Discussion

Examples of the solutions are shown in figures 2, 3, 4 and 5. There is nothing too interesting in the concentration or velocity distributions, and we focus on the interface shape. Figure 2 shows a typical such solution, which shows the slow growth of spatial instability from an initial sinusoidally oscillating interface. For comparison, figure 3 shows growth from a more random initial state, which yields a more spotty growth field. As discussed below, one cannot take a completely random initial state, since this model lacks a high wavenumber smoothing property, and the numerical solution would be unable to proceed in that case.

In seeking to compare our numerical results with the stability analysis, we encounter a problem which in retrospect is not surprising. It is caused by the form of the kinematic equation (2.30) for the interface  $s$ . So long as the normal interface velocity  $v_n = \mathbf{v} \cdot \mathbf{n}$  is given, then (2.30) can be solved by the method of characteristics (cf. Fowler and Winstanley 2012), and if  $v_n > 0$  (which it is certainly is in the one-dimensional solution, see (3.1), and therefore initially), any initially oscillatory interface will have convergent characteristics and thus form cusps; and indeed, this is what happens, and when it does, the solution is singular and our numerical method breaks down.

In more detail, the singularity is manifested as the formation of corners in the biofilm interface. There is nothing intrinsically wrong with the model in this respect: it is quite feasible that the surface  $z = s(x, t)$  should form such kinks. However, our numerical front-fixing method automatically introduces second derivatives of the free surface into the differential equations, and the method consequently breaks down when the first derivatives of  $s$  approach the singularity. A quite different method would be necessary to prolong the numerical solution past this point.

Such an aspiration is beyond the scope of the present study, since we were not even sure that the model would be sufficiently well-posed to have a solution in two dimensions. A simpler alternative is to include an artificial diffusion term  $\delta s_{xx}$  in the kinematic condition, and we have implemented this; the problem then is that this provides a stabilising effect which can remove the instability altogether, unless we choose  $\eta$  to be fairly large. However, such results are difficult to follow, because the method then requires such small time steps that it becomes prohibitive to run long enough.

One simple apparent remedy would be to restrict the initial amplitude  $A$  of the spatial variation of  $s$  to be very small, since we are only really seeking to validate the linear stability result. The problem with this is evident in figure 4. Since the ordinate measures  $\log_{10} A$ , the value of  $\dot{A}/A$  is the slope of the amplitude curves, and is evidently not constant, particularly for the small wave number perturbations. The reason for this is evident in figure 2. Even though the initial mean value of  $s$  is sufficiently large for the one-dimensional solution to be accurate (if  $s$  were constant), the spatial variation already causes a nonlinear adjustment to the growth rate: what we see in figure 4, most obviously at the lowest wave number, is a rapid transient where the growth rate of the mean interface position adapts to its initial distortion, before proceeding to grow pseudo-exponentially. This is why we estimate the slope of

the curves some way beyond the initial transient. On the other hand, we can not go too far, because cusp formation indicates the breakdown of the linear theory. With all these provisos in mind, we consider that the estimated growth rates determined from figure 4 are reasonably in agreement with the theoretical estimate, as shown in figure 5.

## 6 Conclusions

In this paper we have developed the one-dimensional theory for biofilm growth presented by Winstanley *et al.* (2011) to consider solutions which are not laterally uniform. The development and simplification of the model is non-trivial, and it leads to a highly non-standard type of Stokes flow model, whose boundary conditions preclude confidence. Nevertheless, we also develop a direct numerical solution, which shows that a planar interface is unstable, and the results are in satisfactory agreement with a linear stability analysis.

Our analysis also shows, both numerically and analytically, that the interface will develop cusps in finite time. As explained near the beginning of section 5, the formation of cusps is a result of the hyperbolic nature of the kinematic condition (2.49), and we consider this to be a real feature of our model, which unfortunately means that our numerical method which assumes a smooth interface is doomed to fail when the cusps form. Such singularities can be alleviated by incorporating extra physical effects, most notably a surface tension, as was done by Cogan and Keener (2004), but we do not consider that there is any physical justification for such a term, as it would essentially be a surface tension for the polymer matrix. Rather, we tentatively suggest that the formation of cusps in the interface may represent the first steps in our theory of the formation of more exotic, non-smooth architectures, such as are seen experimentally.

We mentioned in the introduction that, broadly, biofilm architectures appear to be favoured in conditions of poor nutrient supply (see for example Heydorn *et al.* (2000)). In order to compare such a statement to our theoretical results, we need to tease apart the dependence of the parameters  $\mu$  and  $\eta$  in (3.27) on the nutrient level  $c_0$  and the transport layer thickness  $d_c$  in (2.12). Low nutrient supply means low  $c_0$  and/or high  $d_c$ . The latter implies high  $\eta$  (see (2.20)), while since in (3.25)  $g = \mu c$  replaces  $g = \frac{c}{c + \kappa}$  in (2.28), we essentially have  $\mu \sim 1/\kappa$ , and since  $\kappa \propto c_0^{-1}$  (Winstanley *et al.* 2011, equation (2.11)), low  $c_0$  means low  $\mu$ .

In figure 6, we plot  $\sigma$  given by (3.27) for three sets of combinations of  $\mu$  and  $\eta$ . Ideally, we would see larger  $\sigma$  for low  $\mu$  and high  $\eta$ , but the opposite conclusion seems to be the case, at least for fixed wave number. However, more important should be the maximum growth rate, and this does not vary very much. Possibly a more robust conclusion from this figure would be that poor nutrient supply favours growth at longer wavelengths, but it may be rash to try and infer too much from such a simple stability theory.

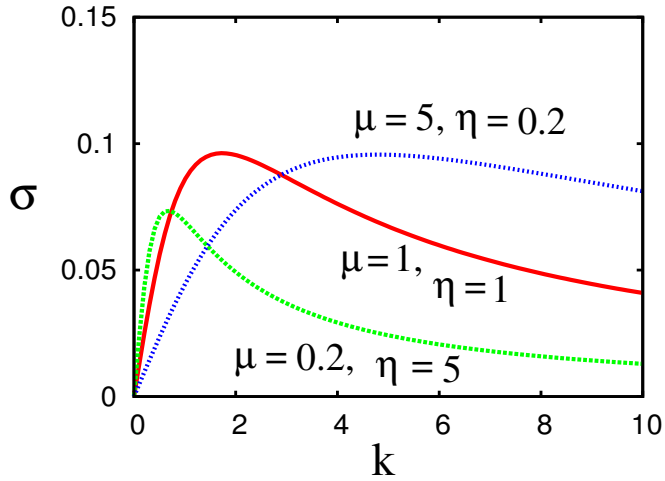


Figure 6: The growth rate  $\sigma(k, \mu, \eta)$  given by (3.27) for values  $\mu = 5, \eta = 0.2$ ;  $\mu = \eta = 1$ ; and  $\mu = 0.2, \eta = 5$  as indicated.

### Data accessibility

The paper contains no data.

### Competing interests

We have no competing interests.

### Authors' contributions

A. C. F. devised and solved the model, and wrote the paper. T. M. K-S. constructed and solved the numerical model. H. F. W. performed the literature review, and assisted with the analytic and numerical work. All authors worked on the final text.

### Acknowledgements

We have no acknowledgements.

### Funding statement

This publication has emanated from research conducted with the financial support of Science Foundation Ireland under grant numbers SFI/09/IN.1/I2645 and SFI/13/IA/1923.

### Ethics statement

This research poses no ethical considerations.

## References

- Balay, S., M.F. Adams, J. Brown, P. Brune, K. Buschelman, V. Eijkhout, W.D. Gropp, D. Kaushik, M.G. Knepley, L.C. McInnes, K. Rupp, B.F. Smith and H. Zhang 2014 PETSc web page: <http://www.mcs.anl.gov/petsc>.
- Balay, S., M.F. Adams, J. Brown, P. Brune, K. Buschelman, V. Eijkhout, W.D. Gropp, D. Kaushik, M.G. Knepley, L.C. McInnes, K. Rupp, B.F. Smith and H. Zhang 2013 PETSc Users Manual. Technical report ANL-95/11 - Revision 3.4, Argonne National Laboratory.
- Balay, S., W.D. Gropp, L.C. McInnes and B.F. Smith 1997 Efficient Management of Parallelism in Object Oriented Numerical Software Libraries. In: *Modern Software Tools in Scientific Computing*, eds. E. Arge, A.M. Bruaset and H. P. Langtangen), Birkhäuser Press, pp. 163–202.
- Batchelor, G.K. 1967 *An introduction to fluid dynamics*. C. U. P., Cambridge.
- Ben Amar, M. and M. Wu 2014 Patterns in biofilms: from contour undulations to fold focussing. *EPL* **108**, 38003.
- Böl, M., A.E. Ehret, A. Bolea Albero, J. Hellriegel, and R. Krull 2013 Recent advances in mechanical characterisation of biofilm and their significance for material modelling. *Critical reviews in biotechnology*, **33** (2), 145–171.
- Cahn, J. W. and J. E. Hilliard 1958 Free energy of a nonuniform system. I. Interfacial free energy. *J. Chem. Phys.* **28**, 2, 258–267.
- Cogan N.G. and J.P. Keener 2004 The role of the biofilm matrix in structural development. *Math. Med. Biol.* **21**, 147–166.
- Costerton, J. W. 2007 *The biofilm primer* (Vol. 1). Springer Science & Business Media.
- Crank, J. 1984 *Free and moving boundary problems*, Clarendon Press.
- Dockery, J. and I. Klapper 2002 Finger formation in biofilm layers. *SIAM J. Appl. Math.* **62**, 853–869.
- Drew, D.A. and S.L. Passman 1999 *Theory of multicomponent fluids*. Springer-Verlag, New York.
- Du, J., R.D. Guy, A.L. Fogelson, G.B. Wright, J.P. Keener 2013 An interface-capturing regularization method for solving the equations for two-fluid mixtures. *Comm. Comp. Phys.* **14**, 1,322–1,346.
- Flory, P.J. 1953 *Principles of polymer chemistry*. Cornell University Press, Cornell.
- Fowler, A.C. and H.F. Winstanley 2012 Movement of a sessile cell colony. *Math. Proc. R. Ir. Acad.* **112A** (2), 79–91.

- Ghosh, P., J. Mondal, E. Ben-Jacob, and H. Levine 2015 Mechanically-driven phase separation in a growing bacterial colony. *PNAS*, E2,166–E2,173.
- Heydorn, A., A. T. Nielsen, M. Hentzer, C. Sternberg, M. Givskov, B. K. Ersbøll, and S. Molin 2000 Quantification of biofilm structures by the novel computer program COMSTAT. *Microbiol.* **146**, 2,395–2,407.
- Kissel, J. C., P. L. McCarty and R. L. Street 1984 Numerical simulation of mixed-culture biofilm. *J. Environ. Engng.* **110**, 393–411.
- Klapper, I. 2012 Productivity and equilibrium in simple biofilm models. *Bull. Math. Biol.* **74**, 2,917–2,934.
- Laspidou, C. S., A. Kungolos, and P. Samaras 2010 Cellular-automata and individual-based approaches for the modeling of biofilm structures: pros and cons. *Desalination*, **250** (1), 390–394.
- Lee, M. W. and J. M. Park 2007 One-dimensional mixed-culture biofilm model considering different space occupancies of particulate components. *Water Research* **41** (19), 4,317–4,328.
- Lindley, B., Q. Wang, and T. Zhang 2012 Multicomponent hydrodynamic model for heterogeneous biofilms: Two-dimensional numerical simulations of growth and interaction with flows. *Physical Review E*, **85** (3), 031908.
- Picioreanu, C., M. C. M. van Loosdrecht and J. J. Heijnen 1998 Mathematical modeling of biofilm structure with a hybrid differential-discrete cellular automaton approach. *Biotechnol. Bioeng.* **58**, 101–116.
- Seminara, A., T. E. Angelini, J. N. Wilking, H. Vlamakis, S. Ebrahim, R. Kolter, D. A. Weitz, and M. P. Brenner 2012 Osmotic spreading of *Bacillus subtilis* biofilms driven by an extracellular matrix. *PNAS*, **109** (4), 1,116–1,121.
- Stoodley, P., R. Cargo, C. J. Rupp, S. Wilson, and I. Klapper 2002 Biofilm material properties as related to shear-induced deformation and detachment phenomena. *J. Ind. Microbiol. Biotechnol.* **29**, 361–367.
- Tiwari, S. K. and K. L. Bowers 2001 Modeling biofilm growth for porous media applications. *Math. Comp. Modelling* **33** (1–3), 299–319.
- Wanner, O. and W. Gujer 1986 A multispecies biofilm model. *Biotechnol. Bioeng.* **28**, 314–328.
- Wanner, O. and P. Reichert 1996 Mathematical modeling of mixed-culture biofilms. *Biotechnol. Bioeng.* **49** (2), 172–184.
- Whitman, W. B., D. C. Coleman, and W. J. Wiebe 1998 Prokaryotes: the unseen majority. *Proc. Nat. Acad. Sci.* **95**, 6,578–6,583.

- Winstanley, H. F. 2011 Mathematical modelling of biofilm growth and bioavailability. D.Phil. thesis, University of Oxford.
- Winstanley, H. F., M. Chapwanya, A.C. Fowler and M.J. McGuinness 2011 A polymer-solvent model of biofilm growth. *Proc. R. Soc. Lond. A* **467**, 1,449–1,467.
- Zhang, T. 2012 Modeling of biocide action against biofilm. *Bull. Math. Biol.*, **74**, 1427–1447.
- Zhang, T., N.G. Cogan, and Q. Wang 2008a Phase field models for biofilms. I. Theory and one-dimensional simulations. *SIAM J. Appl. Math.* **69**, 3, 641–669.
- Zhang, T., N. G. Cogan, and Q. Wang 2008b Phase field models for biofilms. II. 2-D numerical simulations of biofilm-flow interaction. *Commun. Comput. Phys.* **4**, 72–101.